Robotica: (2021) volume 39, pp. 1037–1050. © The Author(s), 2020. Published by Cambridge University Press.
doi:10.1017/S0263574720000880

Motion Control and Trajectory Planning for Obstacle Avoidance of the Mobile Parallel Robot Driven by Three Tracked Vehicles

Shuzhan Shentu†, Fugui Xie†‡, Xin-Jun Liu†‡* and Zhao Gong†

†*The State Key Laboratory of Tribology & Tsinghua University (DME)-Siemens Joint Research Center for Advanced Robotics, Department of Mechanical Engineering (DME), Tsinghua University, Beijing 100084, China. E-mails: stsz17@mails.tsinghua.edu.cn, gongzhao@126.com*
‡*Beijing Key Lab of Precision/Ultra-precision Manufacturing Equipments and Control, Tsinghua University, Beijing 100084, China. E-mail: xiefg@mail.tsinghua.edu.cn*

(Accepted August 12, 2020. First published online: September 11, 2020)

SUMMARY
This paper proposes a mobile parallel robot (MPR) and focuses on obstacle avoidance. When analyzing the collision-free trajectories, the coupling constraints caused by the parallel mechanism and the obstacle should be emphatically solved. The solution is to divide the problem into two steps. First, the genetic algorithm is employed to search and optimize the feasible trajectories under the mechanism constraint of the MPR. Then the trajectory tracking controller is designed to make the tracked vehicles move cooperatively and track a trajectory asymptotically. Finally, simulations and experiments are carried out to verify the effectiveness of the solution.

KEYWORDS: Mobile parallel robot; Trajectory tracking; Trajectory planning; Genetic algorithm; Obstacle avoidance.

1. Introduction

During the past decades, parallel robots have been studied a lot and widely used in many fields.[1–4] Parallel robots have significant advantages such as compact structure, high stiffness, and quick response compared to serial robots,[5] and many interesting parallel robots have been proposed. However, because of the limitation of the joints angles, the workspace of parallel robots is generally smaller than serial robots.[6] To solve the problem, the fixed base is replaced by planar drives or mobile units. The new robots are called mobile parallel robots (MPRs).[7–10] MPR combines the advantages of two kinds of robots, including good flexibility, high stiffness, and increased workspace. However, all the above MPRs can only perform well on the smooth surfaces. In order to work in the rough terrain with sand and gravel, we employed three tracked vehicles as the driving units, and the new MPR with six degrees of freedom is named as VicRoB.[11] Researchers have done much work on MPR, but less attention has been paid to the obstacle avoidance problem. This paper will focus on the problem and give a solution.

The motion of MPR can be considered as a system for there are three mobile units. The problem of multi-vehicle motion has been studied a lot due to its extensive applications with high robustness and engineering application value.[12,13] So far, there have been some common methods such as leader–follower architecture,[14] behavior-based approach,[15] virtual structure,[16] and algebraic graph

* Corresponding author. E-mail: xinjunliu@mail.tsinghua.edu.cn

https://doi.org/10.1017/S0263574720000880 Published online by Cambridge University Press

theory.[17] These traditional methods ensure that each unit is moving toward the designated position to realize formation, and researchers have solved many distributed control problems. Nevertheless, these techniques consider only some specific constraints, so that they are neither appropriate to the situation with physical connection constraints nor the obstacle avoidance problem. New methods have been proposed and attracted much attention in recent years. The distributed receding horizon control,[18] the distributed model predictive control,[19,20] and the protocol in ref.[21] are examples with the advantages of processing the physical constraints explicitly and optimizing the trajectories. They all have the advantages of less computation, low communication cost, and the flexible structure to guarantee the convergence and collision or obstacle avoidance. However, due to the parallel structure, the MPR has coupled constraints. Geometrical parameters of the obstacle, relative positions of vehicles, and workspace of itself will all react to the motion. Compared to other formation forms, three vehicles can only change the relative positions within the workspace through cooperative motion, rather than being completely independent. From this point of view, the obstacle avoidance problem of the MPR is different from the formation of multi-agent systems.

This paper presents a solution that can make full use of the structural characteristics to realize the variable attitude motion and achieve better obstacle avoidance performance. The solution divides the problem into two parts, trajectory tracking and trajectory planning.

On the basis of the coupling constraints and kinematics model of the MPR, the genetic algorithm (GA) is utilized to analyze and plan the suitable trajectories of each tracked vehicle, as the GA is an efficient technique in searching and optimizing the desired trajectory[22] with robustness and simple operating rules. Accordingly, GA considers plenty of solutions at each generation to avoid getting into a local optimal result and is stochastic in selection and reproduction.[16] By employing the GA, all the coupling constraints are taken into account meanwhile. Therefore, the 6-degrees of freedom (DOF) poses adjustment ability of the MPR that can be fully utilized when the vehicles track the trajectories generated by GA.

For trajectory tracking, the kinematics model of tracked vehicles should be considered. Tracked vehicles are the skid-steer mobile units with slipping when traversing general paths, which makes it quite difficult to achieve accurate tracking with the skid-steering kinematics.[23] So we simplify the kinematics model into the two-wheeled differential model. Because of the non-holonomic constraints, Brockett's necessary condition of smooth stabilization is not satisfied.[24] It implicates that there is no smooth or continuous time-invariant static state feedback to make the closed loop stable. There are a number of researches on the tracking control techniques of non-holonomic mobile units at home and abroad.[25,27] Backstepping method is employed here to design a discontinuous trajectory tracking controller for its fast and asymptotically trajectory tracking performance. However, there will be a large position deviation under certain initial errors. In order to deal with this problem, a state machine is introduced to improve the motion controller and construct the closed-loop system with global stability.

The obstacle avoidance method combines with distributed and centralized control. The GA runs in the central control to achieve attitude change of the MPR, taking advantages of the parallel configuration. Then the motion controller works on each vehicle independently to increase efficiency. The rest of the paper is organized as follows. Section 2 gives the inverse solution and the workspace of the MPR. Section 3 designs and optimizes a motion controller based on the backstepping method for the tracked vehicle, which is simplified to the two-wheel differential model. And simulations are carried out to verify the motion controller. Section 4 employs the GA to search the optimal trajectory described by the quartic Bézier curve.

2. Kinematics Analysis of the Mechanism

2.1. Inverse kinematics

The MPR presented in this paper is based on a 3-PPSR (P is prismatic joint; S, spherical joint; R, revolute joint) parallel mechanism consisting of a 6 degrees of freedom moving platform, three links, and three tracked vehicles, as shown in Fig. 1. The links are of fixed length and designed as a triangle to improve the stability of the whole structure. The spherical joints connect the driving units and the

https://doi.org/10.1017/S0263574720000880 Published online by Cambridge University Press

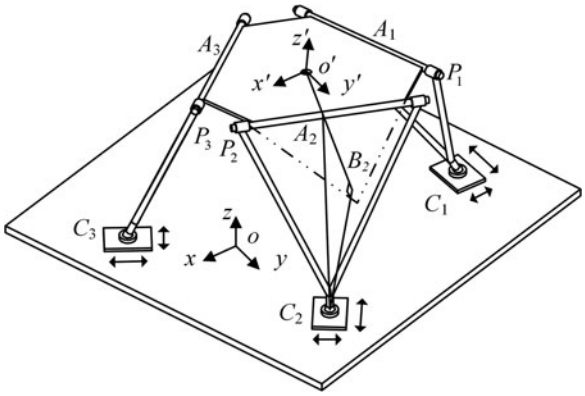


Fig. 1. Parameter description of the kinematic scheme.

lower ends of the links (points C_1,C_2, andC_3). The revolute joints connect the moving platform (sides P_1, P_2, and P_3) and the upper ends of the links. According to the property of parallel mechanisms, the position and attitude of the moving platform are determined by the position of the three spherical joints which are fixed in the driving units.

In Fig. 1, $\{D\}(o' - x'y'z')$ is the moving frame, located at the center of the moving platform o'. The midpoint of the side P_1 is in the negative x-axis, and the z-axis is perpendicular to the moving platform. The global reference frame $\{G\}(o - xyz)$ is attached to the ground. Roll, pitch, and yaw are used to describe the attitude and then it is easy to get the rotation matrix $\boldsymbol{R}$. $\boldsymbol{t} = (x_{o'}, y_{o'}, z_{o'})$ denotes the position coordinate of the point o' in the frame $\{G\}$, and the transform matrices can be expressed by

$$\boldsymbol{T}_D^G = \begin{bmatrix} \boldsymbol{R} & \boldsymbol{t} \\ 0 & 1 \end{bmatrix}, \boldsymbol{T}_G^D = \begin{bmatrix} \boldsymbol{R}^{\mathrm{T}} & -\boldsymbol{R}^{\mathrm{T}}\boldsymbol{t} \\ 0 & 1 \end{bmatrix} \tag{1}$$

where $\boldsymbol{T}_D^G$ means the transform matrix from frame $\{D\}$ to frame $\{G\}$ and $\boldsymbol{T}_G^D$ means the opposite.

The midpoint of the three sides of the platform is defined as $A_i (i = 1, 2, 3)$ and $C_i (i = 1, 2, 3)$ are the centers of the spherical joints which can represent the location of the driving units. The lengths of the lines are expressed by $A_i C_i = 1$, $A_i o' = k$. $B_i C_i (i = 1, 2, 3)$ are the vertical lines from C_i to the moving platform and B_i are the footpoints. Define $\angle B_i A_i C_i = \alpha_i (i = 1, 2, 3)$.

Based on the geometrical conditions of the isosceles triangle and equilateral triangle, it is obvious that $B_i o'$ is vertical to P_i. Then the coordinates of the spherical joints in the moving frame $\{D\}$ can be expressed as

$$C_1' = \begin{bmatrix} -k - l\cos\alpha_1 \\ 0 \\ -l\sin\alpha_1 \end{bmatrix}, C_2' = \begin{bmatrix} 1/2(k + l\cos\alpha_2 \\ \sqrt{3}/2(k + l\cos\alpha_2 \\ -l\sin\alpha_2 \end{bmatrix}, C_3' = \begin{bmatrix} 1/2(k + l\cos\alpha_3 \\ \sqrt{3}/2(k + l\cos\alpha_3 \\ -l\sin\alpha_3 \end{bmatrix} \tag{2}$$

Using the transform matrix T_D^G, the coordinates of C_i in the global reference frame can be obtained by the homogeneous transformation. Considering that all three driving units are on the ground, the z coordinate values of C_i are zero. Hence, three equations about α_i can be expressed as

$$\begin{cases} (-k - l\cos\alpha_1)\, x_k - z_k \cdot l\sin\alpha_1 + z_{o'} = 0 \\ 1/2\,(k + l\cos\alpha_2)\, x_k + \sqrt{3}/2\,(k + l\cos\alpha_2)\, y_k - z_k \cdot l\sin\alpha_2 + z_{o'} = 0 \\ 1/2\,(k + l\cos\alpha_3)\, x_k - \sqrt{3}/2\,(k + l\cos\alpha_3)\, y_k - z_k \cdot l\sin\alpha_3 + z_{o'} = 0 \end{cases} \tag{3}$$

where x_k, y_k, z_k represent the third row of the rotation matrix, respectively.

https://doi.org/10.1017/S0263574720000880 Published online by Cambridge University Press

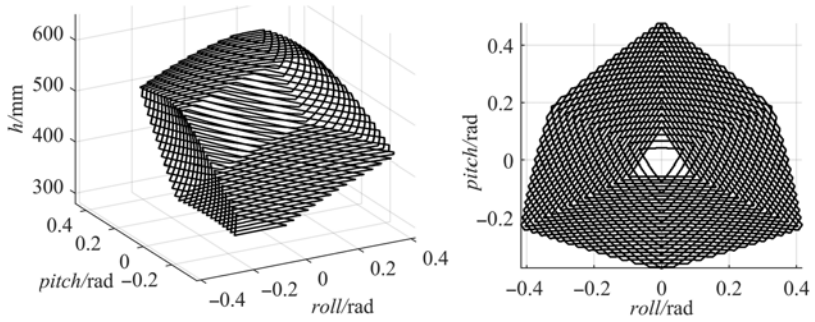


Fig. 2. Workspace at different heights.

By definition, the values of α_i range from 0° to 90°, so there is only one kind of solution of α_i, which can be represented by the given parameters:

$$\begin{aligned}
\alpha_1 &= \sin^{-1}\frac{z_c - kx_k}{l\sqrt{x_k^2 + z_k^2}} - \sin^{-1}\frac{x_k}{\sqrt{x_k^2 + z_k^2}} \\
\alpha_2 &= \sin^{-1}\frac{\frac{1}{2}kx_k + \frac{\sqrt{3}}{2}ky_k + z_c}{\sqrt{\left[\frac{1}{2}l\left(x_k + \sqrt{3}y_k\right)\right]^2 + (lz_k)^2}} + \sin^{-1}\frac{\frac{1}{2}l\left(x_k + \sqrt{3}y_k\right)}{\sqrt{\left[\frac{1}{2}l\left(x_k + \sqrt{3}y_k\right)\right]^2 + (lz_k)^2}} \\
\alpha_3 &= \sin^{-1}\frac{\frac{1}{2}kx_k - \frac{\sqrt{3}}{2}ky_k + z_c}{\sqrt{\left[\frac{1}{2}l\left(x_k - \sqrt{3}y_k\right)\right]^2 + (lz_k)^2}} + \sin^{-1}\frac{\frac{1}{2}l\left(x_k - \sqrt{3}y_k\right)}{\sqrt{\left[\frac{1}{2}l\left(x_k - \sqrt{3}y_k\right)\right]^2 + (lz_k)^2}}
\end{aligned} \tag{4}$$

Through the inverse kinematics solution, if the position and attitude of the moving platform are given, it is feasible to calculate the required positions of three driving units to achieve the target pose of the moving platform.

2.2. *Workspace*

The workspace of a robot is defined as the set of space that the end effector can reach under its structural constraints.[28] And in this work, the end effector is the moving platform. As the MPR can move freely along the x-axis and y-axis directions and rotate around the z-axis, it makes no sense to study these three degrees of freedom. Therefore, the center of the moving platform is kept fixed without yaw and plane motion.

The constraint of the MPR is made up of two aspects. First, the tracked vehicles satisfy the non-holonomic constraints, in which the controllable degree of freedom is less than the total degree of freedom. They need enough space to turn and move to avoid colliding with each other. Second, the angle θ_i between the moving platform and links should be limited from 20° to 80°; otherwise, the robot will have poor kinematic performance or even singular.

Under the circumstances, the workspace with the change of height of the moving platform can be obtained as shown in Fig. 2.

It is easy to observe that the rotation capacity varies from the heights, and there are two extreme values in Fig. 2. To clearly express the workspace of the moving platform at a given height, the tilt and torsion (T&T) angle is employed. Two local maximums of the workspace are in the height of 418 and 551 mm. The workspace represented by the T&T angle is shown in Fig. 3. Then the typical workspace with the h = 500 mm is shown in Fig. 4.

The heavy lines illustrate that the maximum angle the moving platform can reach, and the inner circles of the heavy lines represent the minimum rotation of all directional maxima, respectively. It is obvious that there is a huge difference between the two lines and the workspace is anisotropic in Fig. 3, which is different from the property in Fig. 4. More details about the T&T angle are in ref. [29].

https://doi.org/10.1017/S0263574720000880 Published online by Cambridge University Press

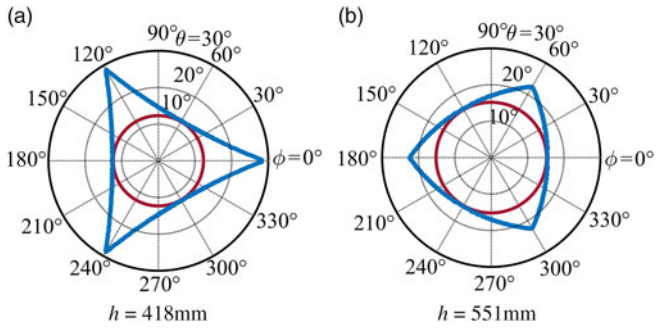


Fig. 3. Workspace of the MPR.

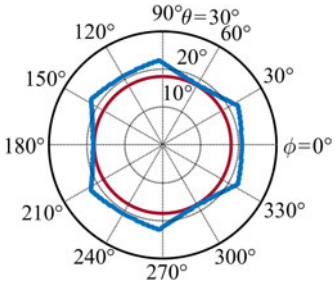


Fig. 4. Workspace of the MPR for $h = 500$ mm.

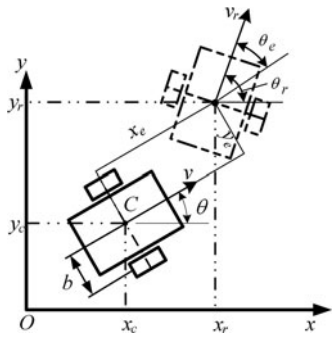


Fig. 5. Trajectory tracking diagram of the tracked vehicle (two-wheeled model).

3. Trajectory Tracking

3.1. Kinematics model of tracked vehicles

Tracked vehicles are simplified into the two-wheeled model as shown in Fig. 5, satisfying the non-holonomic constraints[30] of pure rolling. The velocity of the point C is denoted by v. The radius of the wheel is r, and the distance between two driven wheels is $2b$.

The generalized coordinate $[x, y, \theta]$ is used to describe the model, where (x, y) represents the coordinate of the center point of the tracked vehicle and θ represents the angle between the direction of the chassis and the x-axis. Then the two-wheeled kinematic model can be defined as

$$\begin{cases} \dot{x} = v\cos\theta \\ \dot{y} = v\sin\theta \\ \dot{\theta} = \omega \end{cases} \tag{5}$$

where v and ω represent the linear velocity and angular velocity, respectively, and they are the control inputs of the kinematic model.

https://doi.org/10.1017/S0263574720000880 Published online by Cambridge University Press

3.2. Motion controller design

In this section, a feedback tracking controller is proposed to realize trajectory tracking through the backstepping method.[25,30] For the tracked vehicle, tracking the desired trajectory is equal to following a virtual reference tracked vehicle from the initial position. The trajectory of the reference tracked vehicle is given and the kinematic model also satisfies the non-holonomic constraints represented by (x_r, y_r, θ_r). The system error during following the reference tracked vehicle is demonstrated in Fig. 5.

And its equation is represented as

$$\begin{bmatrix} x_e \\ y_e \\ \theta_e \end{bmatrix} = \begin{bmatrix} \cos\theta & \sin\theta & 0 \\ -\sin\theta & \cos\theta & 0 \\ 0 & 0 & 1 \end{bmatrix} \begin{bmatrix} x_r - x \\ y_r - y \\ \theta_r - \theta \end{bmatrix} \tag{6}$$

Then the differential equation can be got:

$$\begin{bmatrix} \dot{x}_e \\ \dot{y}_e \\ \dot{\theta}_e \end{bmatrix} = \begin{bmatrix} y_e\omega - v + v_r\cos\theta_e \\ -x_e\omega + v_r\sin\theta_e \\ \omega_r - \omega \end{bmatrix} \tag{7}$$

In summary, the motion controller based on the two-wheeled differential drive model is to solve v and ω as the control inputs submitting to the following equation.

$$\lim \left\| \left[x_e, y_e, \theta_e \right]^{\mathrm{T}} \right\| = 0 \tag{8}$$

Of note is that, if $x_e = 0$ and $\theta_e = 0$, $\dot{y}_e = 0$ which means y_e becomes a constant and is uncontrollable. If set $x_e = 0$ and regard θ_e as the virtual control, then y_e can be made asymptotic approach to zero and keep the system stable. So the Lyapunov function candidate V_1 is defined as follows:

$$V_1 = \frac{1}{2} y_e^2 \tag{9}$$

According to Eq. (9), the derivative of Lyapunov function candidate V_1 is

$$\dot{V}_1 = y_e\dot{y}_e = -y_e x_e\omega + y_e v_r \sin\theta_e \tag{10}$$

Considering the intermediate variable $\beta = -\tanh(v_r y_e)$, if $x_e = 0$ and $\theta_e = \beta$, then

$$\dot{V}_1 = y_e v_r \sin\left(-\tanh\left(y_e v_r\right)\right) \tag{11}$$

it is easy to prove that $\dot{V}_1 \leq 0$ and the function illustrates that y_e is the asymptotic approach to zero when $x_e = 0$ and $\theta_e = \beta = -\tanh(v_r y_e)$. β is a intermediate variable. Therefore, let us introduce a new variable $\bar{\theta}_e = \theta_e - \beta$. Select x_e, y_e and $\bar{\theta}_e$ as the new control variables. In terms of V_1, the Lyapunov function V_2 can be defined as

$$V_2 = V_1 + \frac{1}{2}x_e^2 + \left(1 - \cos\frac{\bar{\theta}_e}{2}\right) = \frac{1}{2}y_e^2 + \frac{1}{2}x_e^2 + \left(1 - \cos\frac{\bar{\theta}_e}{2}\right) > 0 \tag{12}$$

The derivative of the above function is,

$$\dot{V}_2 = x_e\left(-v + v_r\cos\theta_e\right) + y_e v_r\sin\theta_e + \frac{1}{2}\sin\frac{\bar{\theta}_e}{2}\left(\omega_r - \omega + x_e\omega\frac{\partial\beta}{\partial y_e} - \dot{v}_r\frac{\partial\beta}{\partial v_r} - v_r\sin\theta_e\frac{\partial\beta}{\partial y_e}\right) \tag{13}$$

which can be transformed into

$$y_e v_r\sin\theta_e = 2y_e v_r\sin\frac{\bar{\theta}_e}{2}\cos\left(\frac{\bar{\theta}_e}{2} + \beta\right) + y_e v_r\sin\beta \tag{14}$$

https://doi.org/10.1017/S0263574720000880 Published online by Cambridge University Press

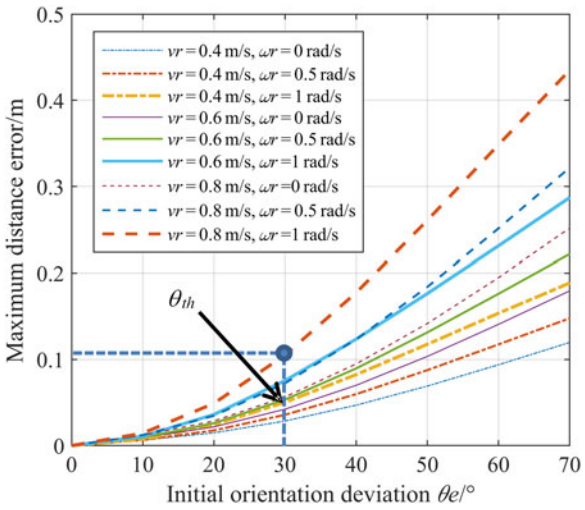


Fig. 6. Maximum distance error at different initial angles.

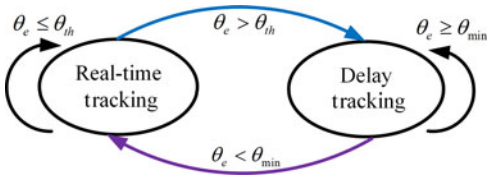


Fig. 7. Schematic diagram of the state machine.

Rewrite the Eq. (13) using the velocity v and ω as the independent variable. On the basis of the Lyapunov stability theory, the system shows asymptotic stability when $\dot{V}_2 \leq 0$. According to Eq. (11), $y_e y_r \sin\beta \leq 0$. So the motion controller can be writen as

$$\begin{cases} v = v_r \cos\theta_e + \dfrac{\omega}{2} \sin\dfrac{\bar{\theta}_e}{2} \cdot \dfrac{\partial\beta}{\partial y_e} + k_1 x_e \\ \omega = \omega_r - \dfrac{\partial\beta}{\partial y_e} \cdot v_r \sin\theta_e - \dfrac{\partial\beta}{\partial v_r} \cdot v_r + 4 y_e y_r \cos\left(\dfrac{\bar{\theta}_e}{2} + \beta\right) + k_2 \sin\dfrac{\bar{\theta}_e}{2} \end{cases} \tag{15}$$

where v and ω are the control inputs of the kinematics model and k_1, k_2 are positive constant gains. Combined with the velocity of two wheels (v_1 represents the left and v_2 is the right), the controller of them is

$$\begin{cases} v_1 = v + b\omega \\ v_2 = v - b\omega \end{cases} \tag{16}$$

3.3. Motion controller optimized

The kinematics model of the tracked vehicle is a non-holonomic constraint model. This will result in that the motion controller will have a large position error, even bigger than the initial error when the initial orientation deviation is large. The maximum position errors (the initial position error is zero) under different initial orientation deviation are shown in Fig. 6. As the initial orientation deviation increases, the configuration control of the tracked vehicle is less accurate, even though the system eventually turns to stabilize.

For better motion control, a state machine is introduced in Fig. 7 to avoid the situation. The optimized trajectory tracking controller should have two states, switched by the state machine. θ_{th} is the threshold value, equaling to 30°, to determine the state. $\theta_{\min}$ is the value of the target tracking error. θ_e represents the orientation deviation at this moment.

https://doi.org/10.1017/S0263574720000880 Published online by Cambridge University Press

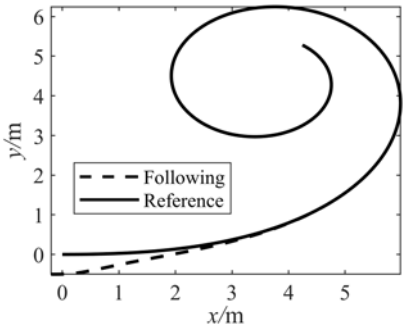


Fig. 8. Trajectory tracking 1.

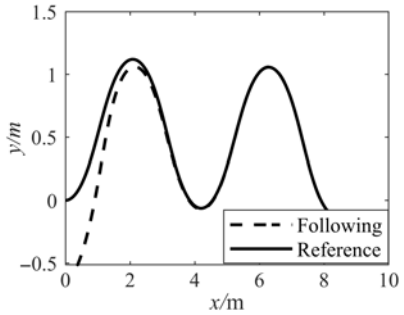


Fig. 9. Trajectory tracking 2.

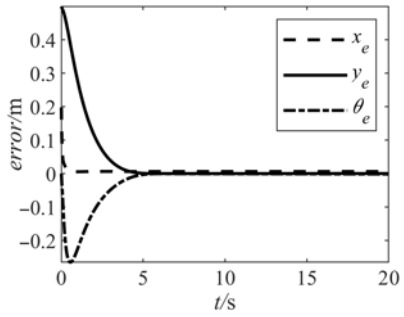


Fig. 10. Trajectory tracking errors 1.

One is real-time tracking designed by the backstepping method, as described in the previous section, which makes (x_e, y_e, θ_e) approach to (0, 0, 0) directly.

The other is delay tracking, which means the virtual tracked vehicle stays where it is and turns to track the angle first. Then the motion controller realizes (x_e, y_e) approaching to (0, 0) by real-time tracking.

The initial orientation deviation cannot be avoided and predicted in practice. Hence, it is meaningful to introduce a state machine to solve this problem.

3.4. Simulations of the motion controller

To verify the performance of the motion controller, simulations are employed to demonstrate the results of trajectory tracking. The maximum velocities are set as $v_{\max} = 0.8$ m/s and $\omega_{\max} = 1$ rad/s. The initial position of reference tracked vehicle is set as $\left[x_r, y_r, \theta_r\right] = [0, 0, 0]$, and the sampling frequency of the system is $f = 100$ Hz. The two positive constant parameters are essential to the motion controller. $k_1 = 24$ and $k_2 = 8$ are selected through simple analysis and simulations.

In simulation 1, the reference velocity is $v_r = 0.8$ m/s and $\omega_r = 0.04\,(t + 1)$ rad/s $(t \in [0, 20])$ with the initial error $[x_e, y_e, \theta_e] = [-0.2, 0.5, 0]$. In simulation 2, the reference velocity $v_r = 0.8$ m/s and $\omega_r = \cos(4t/\pi)$ rad/s with the initial error $[x_e, y_e, \theta_e] = [-0.1, 0.6, \pi/6]$. Figures 8 and 9 show the trajectory tracking. Figures 10 and 11 imply tracking errors.

https://doi.org/10.1017/S0263574720000880 Published online by Cambridge University Press

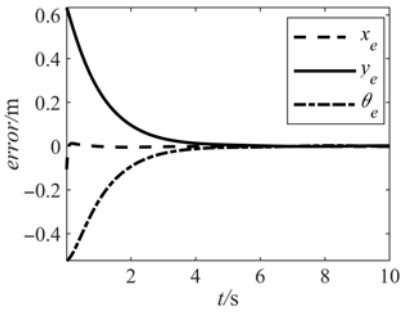


Fig. 11. Trajectory tracking errors 2.

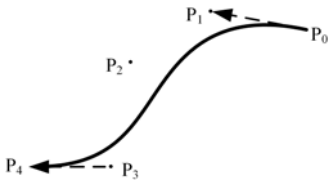


Fig. 12. Example of the quartic Bézier curve.

Analyzing the simulation results, it is obvious that the motion controller is effective in trajectory tracking. The motion controller has reduced the chattering and provided good tracking, even though there are different initial position errors or orientation deviation.

4. Trajectory Planning

For the MPR, there are two ways to avoid the obstacle for the VicRoB. First, three tracked vehicles can move on the same side of the obstacle to avoid it on the condition that there is enough space. Second, three tracked vehicles move cooperatively to cross over the obstacle and under the moving platform. This section will focus on the second situation and put forward a trajectory planning method to take full advantage of the internal space of the robot.

4.1. Quartic Bézier curve and mathematical model

The trajectory planning method is based on the quartic Bézier curve as shown in Fig. 12. A planar quartic Bézier curve is only defined by five control points $P_i = (x_{p_i}, y_{p_i})(i = 1, 2, 3, 4, 5)$ without passing through all the data points.[31] The advantages include that the Bézier curves start at P_0 and end at P_4, the radius of curvature varies smoothly from P_0 to P_4 for its continuous higher order derivatives, and the vector tangential at the start (end) is along the vectors $\boldsymbol{P_1P_2}$ ($\boldsymbol{P_3P_4}$),[32,33] which are essential to generate the trajectory.

The parametric formulation of the quartic Bézier curve is:

$$\begin{cases} x(t) = x_{p_0}(1-t)^4 + 4x_{p_1}(1-t)^3\, t + 6x_{p_2}(1-t)^2\, t^2 + 4x_{p_3}(1-t)\, t^3 + x_{p_4}t^4 \\ y\,(t) = y_{p_0}(1-t)^4 + 4y_{p_1}(1-t)^3\, t + 6y_{p_2}(1-t)^2\, t^2 + 4y_{p_3}(1-t)\, t^3 + y_{p_4}t^4 \end{cases} \tag{17}$$

where t is a parameter and $t \in [0, 1]$. The curvature is formulated by

$$\kappa(t) = \frac{x'(t)\, y''(t) - y'(t)\, x''(t)}{\left(x'^2\,(t) + y'^2\,(t)\right)^{\frac{3}{2}}} \tag{18}$$

In order to ensure that the steering angle θ is continuous, the curvature $\kappa(t)$ has to be continuous. It is obvious that the discontinuous trajectory curvature only occurs when

$$x'(t) = y'(t) = 0 \tag{19}$$

This situation will lead to the curve interrupt at this point, totally opposite the property of the curve.

https://doi.org/10.1017/S0263574720000880 Published online by Cambridge University Press

Since the quartic Bézier curve is invariance under affine transformation, the problem will not change if the initial orientation is rotated parallel to the x-axis. Suppose $|P_0P_1| = |P_3P_4| = d$ and keep the terminal velocity the same to the initial direction. Then, the coordinates of P_1 and P_3 are realized:

$$P_1 = \left(x_{P_0} - d,\, y_{P_0}\right),\; P_3 = \left(x_{P_4} + d,\, y_{P_4}\right) \tag{20}$$

Only the related properties of the quartic Bézier curve are explained, and the detailed contents are referred in ref. [34].

4.2. Trajectory planning by genetic algorithm

The GA is adopted to plan the trajectory, aiming to provide a collision free with an obstacle, the minimum cost of the motion, and shortest trajectory. For the trajectory, the parameters to optimize include x_{p_0}, y_{p_0}, x_{p_2}, y_{p_2}, x_{p_4}, x_{p_4}, and d. In the obstacle avoidance work, there is no precise starting position or target position but a feasible scope instead. Combined with the characteristics of the problem, the fitness function is defined as

$$f = (u_1 f_1 + u_2 f_2 + u_3 f_3) \cdot f_4 \tag{21}$$

In this function,

f: Gene fitness value;
f_1: Minimum distance between three tracked vehicles and obstacles;
f_2: Distance of the trajectory;
f_3: Attitude change of the moving platform;
f_4: Interference index, if interference $f_4 = 0$, else $f_4 = 1$;
u_1, u_2, u_3: Weight coefficient.

It is easy to understand f_1 and f_2, but in actual operations, it is impossible to calculate every point on the curve. Hence, dividing the parameter t into 500 parts to describe f_1 and f_2. The expressions of each fitness value are defined as

$$\begin{aligned} f_1 &= \min(\min d_i) - l_1 \\ f_2 &= 1/\left(\sum dist_i - l_2\right) \\ f_3 &= 1/\left(\max(q) - \min(q) + 1\right) \end{aligned} \tag{22}$$

where d_i is the distance between the tracked vehicle and obstacle of the track i, $\Sigma dist_i$ is the sum of the lengths of 500 parts, and q represents the attitude change of the moving platform for all the feasible attitudes that have been calculated in Section 2.2 and stored in the matrix. l_1 and l_2 are two constants to make the differences among fitness values more obvious. As an example, there are two tracks with $\sum dist_i$ equaling 3200 and 3400 mm, it is hard to distinguish them when $f_2 = 1/\sum dist_i$, even though the weight coefficient u_2 is big. But if k_2 is added in the function and equals 2800, this problem no longer occurs. And so does k_1.

The fitness value indicates the quality of the chromosome. Individuals with higher fitness values perform better than the lower ones. For the GA, the way to judge whether the parameters are optimized is if the fitness values of all the chromosomes are close, it illustrates we can quit the program and get the optimized solution, otherwise, the GA program keeps running. The flow chart of the GA is shown in Fig. 13.

The genetic operators of the chromosomes have three parts. The roulette wheel selection is employed here as the selection operator.[35] One point crossover operator (P_c) is used in order to ensure the diversity of the chromosomes and avoid damaging the good genotype.

The mutation is hard to control and usually the probability of occurrence P_m is low, but it is of importance to the evolution. If every gene in a chromosome is represented by four bits code and only has single number 1 or 0 like 0000:1111:0000, the individual's performance is not good since the control points are all at the edge of the region. For this situation, the mutation probability greatly increases to $P_{m'} = 0.2$, called "Effective mutation."

https://doi.org/10.1017/S0263574720000880 Published online by Cambridge University Press

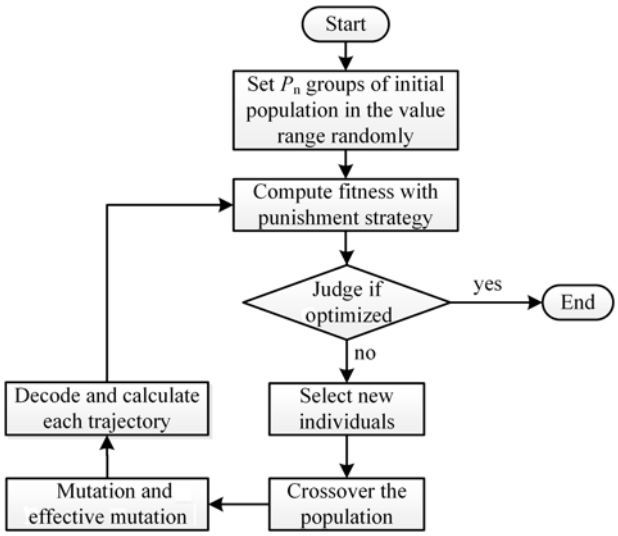


Fig. 13. The flow chart of the genetic algorithm.

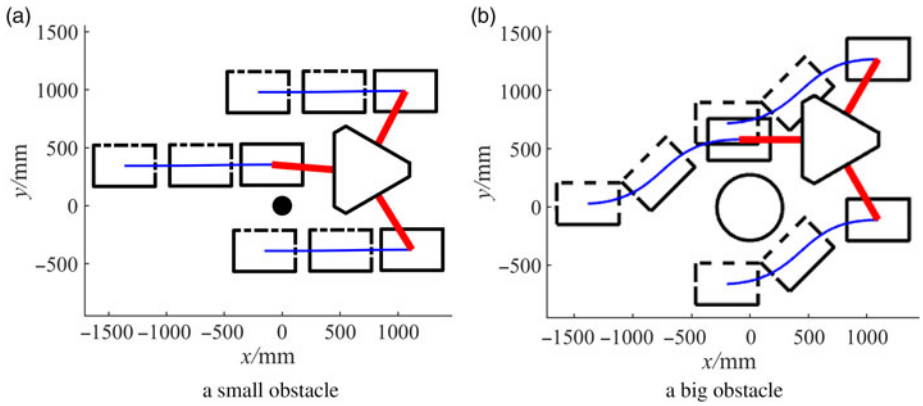


Fig. 14. Experiments results of crossing obstacle.

As the program runs, there will be some chromosomes with zero fitness value, which means the paths are infeasible and interference with the obstacles. These chromosomes will make the variance large. The way to deal with the infeasible chromosomes is through the punishment strategy to delete them and generate new populations into P_n groups from the rest of the chromosomes randomly.

From the analysis in Section 2.2, we know that the workspace is related to heights. If the obstacle height is h, before the program runs, the most suitable height of the moving platform is selected to simplify the problem. Consequently, the model of the tracked vehicle is regarded as a circle with $r_c = 260$ mm, and the radius of the minimum envelope circle of the obstacle is r_0. If the radius of the tracked vehicle transfer into the obstacle, the obstacle is enlarged by $r = r_o + r_c$. Thus, the interference judgment is transformed into the position relation between a point and a circle. This method can greatly reduce the amount of calculation and is widely used in practical obstacle avoidance work, although this simplification wastes part of the workspace.[36]

4.3. Trajectory planning results

The initial probabilities of the operators are selected as $P_c = 0.6$, $P_m = 0.05$ (effective mutation $P_{m'} = 0.2$), and the population size $P_n = 500$. The weight coefficients are $u_1 = 0.12$, $u_2 = 15$, $u_3 = 3000$ to make three fitness values in the same order of magnitude with discrimination, and the weight coefficients are adjusted according to the importance. The results are demonstrated in Fig. 14.

The two figures, respectively, represent the trajectory when crossing different obstacles (circle in the middle) with $r_c = 100$ mm and $r_c = 280$ mm. Seven parameters are optimized within a definite range of values. The hexagon and the rectangles are the platform and tracked vehicles, respectively.

https://doi.org/10.1017/S0263574720000880 Published online by Cambridge University Press

Table I. Iterative results of genetic algorithm.

Generation	20	40	80	120	160	200
Fitness value	98.39	99.11	100.66	101.45	101.50	101.51
Variance	23.34	16.64	15.84	14.26	7.61	7.56

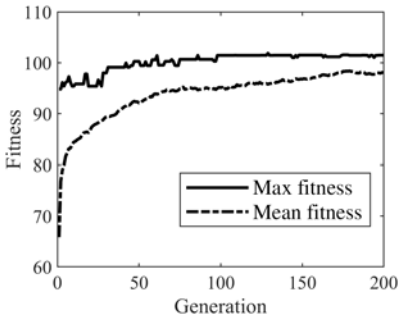


Fig. 15. Fitness value over generations.

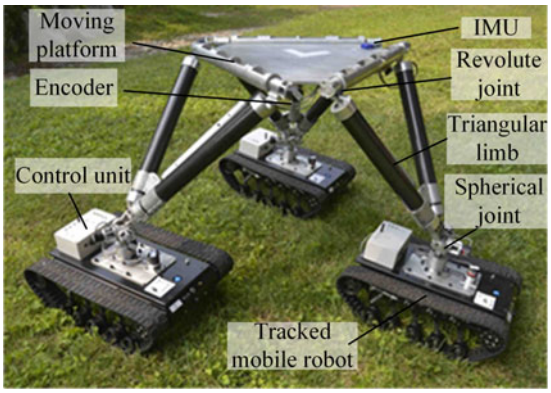


Fig. 16. The prototype of VicRoB.

The heavy lines between them are links. The full line rectangles are in the initial positions, and the middle and the end positions are represented by the dotted line rectangles. Three tracked vehicles move along the fine lines, which represent the trajectories. The trajectory is totally different for various sizes of obstacles, including the initial positions, attitude changes, and the minimum distance. Table I illustrates the iterative results of GA with $r_c = 280$ mm, and Fig. 15 signifies the changing situation of fitness values over generations.

Obviously, the mean fitness increases rapidly in the first 50 generations, indicating the selection operation and punishment strategy performs well. Meanwhile, the optimal solution appears less than generation 120 with a pretty fast convergence speed, which takes a short time to finish the searching program. And the max fitness changes because crossover and mutation are occurring randomly, but the fitness value basically remains a balanced state. Overall, this result indicates the goal of optimizing trajectory is reached by the GA.

4.4. Experiment

The new MPR (called VicRoB) is designed as shown in Fig. 16, consisting of a moving platform, three triangular limbs, and three tracked vehicles. More detailed information about VicRoB is in ref. [11]. An inertial measurement unit is used for calculating the attitude. Additionally, 12 optical encoders are equipped to get position relations between the moving platform and tracked vehicles, and the scanning frequency is 20 Hz.

The experiment was carried out in the laboratory. The position of the robot is calculated by adopting the time difference of arrival based on ultra wideband. Four positioning base stations are fixed at a certain distance from the corners, and the tag is fixed on the moving platform, connecting to the

https://doi.org/10.1017/S0263574720000880 Published online by Cambridge University Press

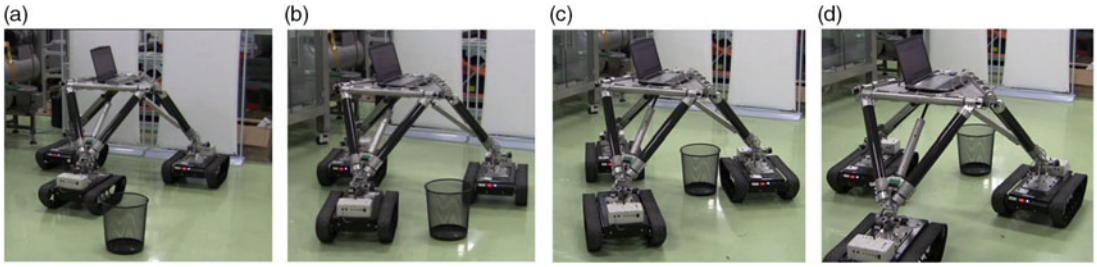


Fig. 17. The process of obstacle crossing experiment.

laptop. The position coordinate of the obstacle is (0, 0), and the VicRoB is placed at (–1600, 600). As mentioned in Section 4.2, the height of the obstacle is 400 mm, so 500 mm is selected as the input height and the initial attitude is horizontal.

According to the information above, the control algorithm works in the following way. When the position of the obstacle is given, the trajectories of three vehicles are calculated in the laptop, connected with the central controller. GA is employed to optimize the trajectories under coupling constraints and kinetic characteristics. The central controller inputs the respective trajectory to the control unit. Each vehicle moves independently along their own trajectory. If a vehicle deviates from the assumed trajectories, the central controller can calculate the error through 12 encoders. Then, it will send the control instructions to the distributed control unit to drive the vehicle back to the trajectory. The central controller and the control units are in one-way communication to decrease the communication cost.

The process of obstacle avoiding is demonstrated in Fig. 17. The robot is in the initial position as shown in Fig. 17(a), then moves across the obstacle in (b) and (c) and arrives at the terminal in (d).

5. Conclusion

In this paper, a control method is proposed to solve the cooperative motion and obstacle avoidance problem of the new kind of MPR. Aiming at the complex coupling constraints and kinetic characteristics, the GA is employed to make the MPR more flexible. By determining the fitness function and improving the algorithm, the optimized trajectories based on the Bézier curve are selected to ensure the process of obstacle avoidance. In order to guarantee the stability of the whole robot, a motion controller is designed to keep each vehicle move synchronously and track the trajectories. The motion controller adjusts the input according to the motion errors in real time, and a state machine is designed to decrease the tracking error. The GA and error detection are performed in the central controller to realize the overall planning, while the motion controller is distributed, and efficiency is improved in this way. Simulations and experiments are carried out to present the effectiveness of the control method, which can give full play to the structural characteristics, realize the variable attitude movement, and avoid obstacles.

Acknowledgments

This work was supported by the National Natural Science Foundation of China under Grants 91748205 and 91948301.

References

1. Y. Lu, Y. Liu, L. Zhang, N. Ye and Y. Wang, "Dynamics analysis of a novel 5-DoF parallel manipulator with couple-constrained wrench," *Robotica* **36**(10), 1421–1435 (2016).
2. F. G. Xie, X.-J. Liu, C. Wu and P. Zhang, "A novel spray painting robotic device for the coating process in automotive industry," *Proc. Inst. Mech. Eng. C: J. Mech. Eng. Sci.* **229**(11), 2081–2093 (2015).
3. J. Mo, Z. F. Shao, L. Guan, F. G. Xie and X. Q. Tang, "Dynamic performance analysis of the X4 high-speed pick-and-place parallel robot," *Robot. Comput.-Integr. Manuf.* **46**, 48–57 (2017).
4. A. S. Lafmejani, M. T. Masouleh and A. Kalhor, "Trajectory tracking control of a pneumatically actuated 6-DOF Gough–Stewart parallel robot using Backstepping-Sliding Mode controller and geometry-based quasi forward kinematic method," *Robot. Comput.-Integr. Manuf.* **54**, 96–114 (2018).
5. X. Chen, X.-J. Liu and F. G. Xie, "Screw theory based singularity analysis of lower-mobility parallel robots considering the motion/force transmissibility and constrainability," *Math. Prob. Eng.* **2015**, 1–11 (2015).
6. J. S. Wang, X.-J. Liu and C. Wu, "Optimal design of a new spatial 3-DOF parallel robot with respect to a frame-free index," *Sci. Chin. Ser. E: Technol. Sci.* **52**(4), 986–999 (2009).

https://doi.org/10.1017/S0263574720000880 Published online by Cambridge University Press

7. W. Kuhlbusch, W. Moritz, J. Lückel and S. Toepper, "TriPlanar-A new parallel 6-DOF robot for highly precise measurement and process tasks," *IFAC Proc. Vol.* **33**(26), 463–467 (2000).
8. F. Tahmasebi and L. W. Tsai, "Closed-form direct kinematics solution of a new parallel minimanipulator," *J. Mech. Des.* **116**(4), 1141–1147 (1994).
9. R. Ben-Horin, M. Shoham and S. Djerassi, "Kinematics, dynamics and construction of a planarly actuated parallel robot," *Robot. Comput.-Integr. Manuf.* **14**(2), 163–172 (1998).
10. Y. Hu, J. Zhang, Z. Wan and J. Lin, "Design and analysis of a 6-DOF mobile parallel robot with 3 limbs," *J. Mech. Sci. Technol.* **25**(12), 3215–3222 (2011).
11. X.-J. Liu, Z. Gong, F. G. Xie and S. Z. Shentu, "Kinematics Analysis and Motion Control of a Mobile Robot Driven by Three Tracked Vehicles," **In:** *ASME 2018 International Design Engineering Technical Conferences and Computers and Information in Engineering Conference* (2018) pp. V05AT07A068–V05AT07A068.
12. V. Sathiya and M. Chinnadurai, "Evolutionary algorithms-based multi-objective optimal mobile robot trajectory planning," *Robotica* **37**(8), 1363–1382 (2019).
13. X. Chu, Z. Peng, G. Wen and A. Rahmani, "Distributed fixed-time formation tracking of multi-robot systems with nonholonomic constraints," *Neurocomputing* **313**, 167–174 (2018).
14. R. Fierro, A. K. Das, V. Kumar and J. P. Ostrowski, "Hybrid Control of Formations of Robots," *Proceedings 2001 ICRA, IEEE International Conference on Robotics and Automation,* Vol. 1 (Cat. No. 01CH37164), (2001) pp. 157–162.
15. J. R. Lawton, R. W. Beard and B. J. Young, "A decentralized approach to formation maneuvers," *IEEE Trans. Robot. Autom.* **19**(6), 933–941 (2003).
16. A. Abbaspour, K. Alipour, H. Z. Jafari and S. A. Moosavian, "Optimal formation and control of cooperative wheeled mobile robots," *Comptes Rendus Mécanique* **343**(5–6), 307–321 (2015).
17. B. D. Anderson, C. Yu, B. Fidan and J. M. Hendrickx, "Rigid graph control architectures for autonomous formations," *IEEE Cont. Syst. Mag.* **28**(6), 48–63 (2008).
18. P. Wang and B. Ding, "Distributed RHC for tracking and formation of nonholonomic multi-vehicle systems," *IEEE Trans. Autom. Cont.* **59**(6), 1439–1453 (2014).
19. L. Dai, Q. Cao, Y. Xia and Y Gao, "Distributed MPC for formation of multi-agent systems with collision avoidance and obstacle avoidance," *J. Franklin Inst.* **354**(4), 2068–2085 (2017).
20. P. U. Lima, A. Ahmad, A. Dias, A. G. Conceição, A. P. Moreira, E. Silva and T. P. Nascimento, "Formation control driven by cooperative object tracking," *Robot. Autonom. Syst.* **63**, 68–79 (2015).
21. S. De, S. R. Sahoo and P. Wahi, "Trajectory tracking control with heterogeneous input delay in multi-agent system," *J. Intell. Robot. Syst.* **92**(3–4), 521–544 (2018).
22. Y. H. Gan and X. Z. Dai, "Optimal trajectory-planning based on genetic algorithm for multi-robot system.," *Cont. Theory Appl.* **27**(9), 1245–1252 (2010).
23. T. Zou, J. Angeles and F. Hassani, "Dynamic modeling and trajectory tracking control of unmanned tracked vehicles," *Robot. Autonom. Syst.* **110**, 102–111 (2018).
24. M. Sarfraz and F. U. Rehman, "Feedback stabilization of nonholonomic drift-free systems using adaptive integral sliding mode control," *Arab. J. Sci. Eng.* **42**(7), 2787–2797 (2017).
25. A. Mustafa, N. K. Dhar, P. Agrawal and N. K. Yerma, "Adaptive Backstepping Sliding Mode Control Based on Nonlinear Disturbance Observer for Trajectory Tracking of Robotic Manipulator," **In:** *2017 2nd International Conference on Control and Robotics Engineering (ICCRE)* (2017) pp. 29–34.
26. M. E. Serrano, S. A. Godoy, V. A. Mut, O. A. Ortiz and G. J. Scaglia, "A nonlinear trajectory tracking controller for mobile robots with velocity limitation via parameters regulation," *Robotica* **34**(11), 2546–2565 (2016).
27. R. Fareh, M. R. Saad, M. Saad, A. Brahmi and M. Bettayeb, "Trajectory tracking and stability analysis for mobile manipulators based on decentralized control," *Robotica* **37**(10), 1–18 (2019).
28. J. Fu and F. Gao, "Optimal design of a 3-leg 6-DOF parallel manipulator for a specific workspace," *Chin. J. Mech. Eng.* **29**(4), 659–668 (2016).
29. I. A. Bonev, *Geometric Analysis of Parallel Mechanisms* (Université Laval, Canada, 2002).
30. J. T. Huang and Y. L. Sung, "Adaptive Beckstepping Dynamic Surface Tracking Control of Nonholonomic Mobile Robots," **In:** *2016 IEEE 11th Conference on Industrial Electronics and Applications (ICIEA)* (2016) pp. 1026–1031.
31. C. Chen, Y. He, C. Bu, J. Han and X. Zhang, "Quartic Bézier Curve Based Trajectory Generation for Autonomous Vehicles with Curvature and Velocity Constraints," **In:** *2014 IEEE International Conference on Robotics and Automation (ICRA)* (2014) pp. 6108–6113.
32. K. G. Jolly, R. S. Kumar and R. Vijayakumar, "A Bezier curve based path planning in a multi-agent robot soccer system without violating the acceleration limits," *Robotics and Autonomous Systems* **57**(1), 23–33 (2009).
33. K. R. Simba, N. Uchiyama and S. Sano, "Real-time smooth trajectory generation for nonholonomic mobile robots using Bézier curves," *Robot. Comput.-Integr. Manuf.* **41**, 31–42 (2016).
34. D. Marsh, *Applied Geometry for Computer Graphics and CAD* (Springer Science & Business Media, Berlin, Germany, 2006).
35. Y. Qu, Y. Zhang and Y. Zhang, "A global path planning algorithm for fixed-wing UAVs," *J. Intell. Robot. Syst.* **91**(3–4), 691–707 (2018).
36. R. Qi, W. Zhou and T. Wang, "An obstacle avoidance trajectory planning scheme for space manipulators based on genetic algorithm," *Robot* **36**(3), 263–270 (2014).

https://doi.org/10.1017/S0263574720000880 Published online by Cambridge University Press